

Batteries & Supercaps

Supporting Information

Effect of Presodiation Additive on Structural and Interfacial Stability of Hard Carbon | P2-Na_{0.66}Mn_{0.75}Ni_{0.2}Mg_{0.05}O₂ Full Cell

Leonardo Sbrascini, Angelina Sarapulova, Cornelius Gauckler, Lydia Gehrlein, Fabian Jeschull, Tolga Akçay, Reiner Mönig, Mario Marinaro,* Francesco Nobili,* and Sonia Dsoke*

Effect of Presodiation Additive on Structural and Interfacial Stability of P2-Na_{0.66}Mn_{0.75}Ni_{0.2}Mg_{0.05}O₂/Hard Carbon Full Cell

Leonardo Sbrascini^[a], Angelina Sarapulova^[b], Cornelius Gauckler^[c], Lydia Gehrlein^[b], Fabian Jeschull^[b], Tolga Akçay^[b], Reiner Mönig^[b], Mario Marinaro^{*[c]}, Francesco Nobili^{*[a],[d]}, Sonia Dsoke^{*[b],[e],[f]}

- [a] L. Sbrascini, F. Nobili
School of Science and Technologies – Chemistry Division
University of Camerino
Via Madonna delle Carceri – CHIP, Camerino 62032, Italy
E-mail: francesco.nobili@unicam.it
- [b] A. Sarapulova, L. Gehrlein, F. Jeschull, T. Akçay, R. Mönig, S. Dsoke,
Institute for Applied Materials (IAM)
Karlsruhe Institute of Technology (KIT)
Hermann-von-Helmholtz-Platz 1, D-76344 Eggenstein-Leopoldshafen, Germany
- [c] C. Gauckler, M. Marinaro
Zentrum Für Sonnenenergie Und Wasserstoff Forschung Baden-Württemberg (ZSW)
Helmholtzstraße 8, 89081 Ulm (Germany)
E-mail: mario.marinaro@zsw-bw.de
- [d] F. Nobili
GISEL – Centro di Riferimento Nazionale per i Sistemi di Accumulo Elettrochimico di Energia
INSTM, Firenze 50121, Italy
- [e] S. Dsoke
Albert-Ludwigs-University Freiburg, Department of Sustainable Systems Engineering (INATECH)
Emmy-Noether-Straße 2, 79110, Freiburg, Germany
E-mail: sonia.dsoke@inatech.uni-freiburg.de
- [f] S. Dsoke
Fraunhofer Institute for Solar Energy Systems, Dep. Electrical Energy Storage
Heidenhofstr 2, 79110 Freiburg, Germany

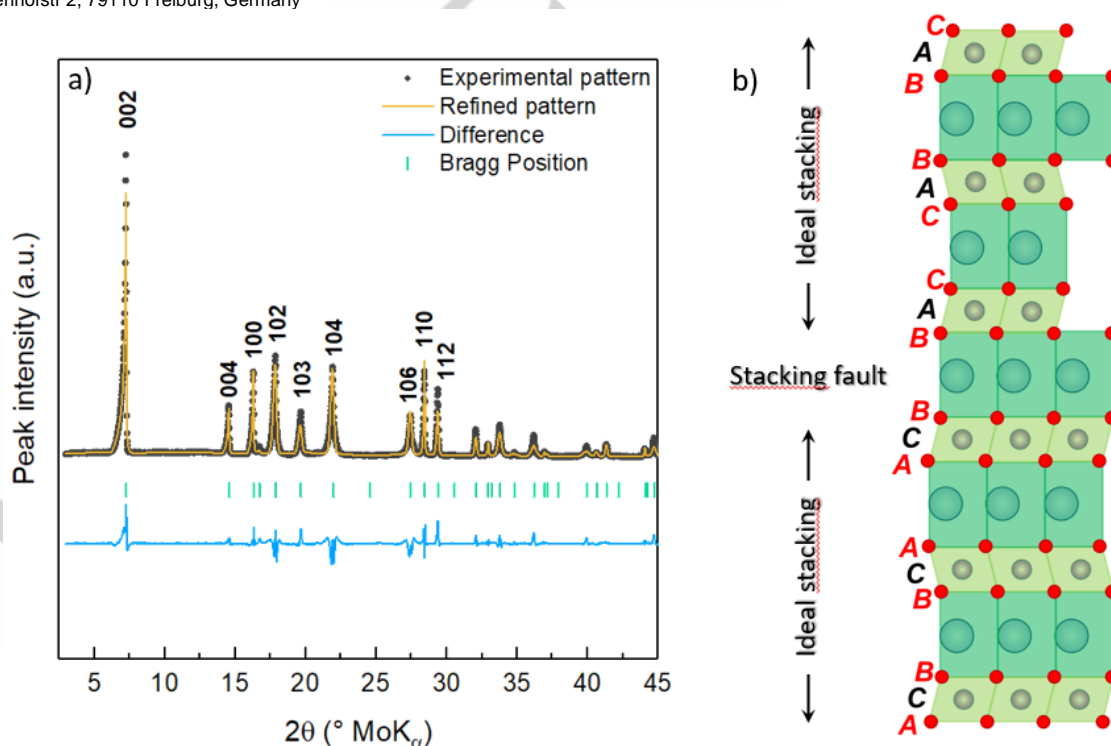


Figure S1. a) Diffraction pattern and Rietveld refinement from XRD data for P2-NaMnMO; b) Schematic representation of the stacking fault sequence.

Lattice parameters: $a = 2.886 \text{ \AA}$; $c = 11.183 \text{ \AA}$.

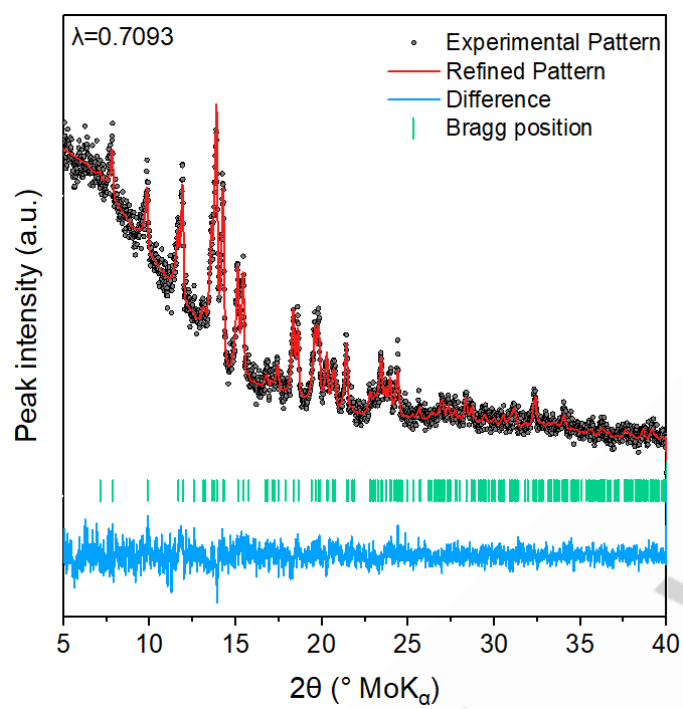


Figure S2. Diffraction pattern and Rietveld refinement from XRD data for $\text{Na}_2\text{C}_4\text{O}_4$

Lattice parameters: $a = 3.493 \text{ \AA}$; $b = 6.823 \text{ \AA}$; $c = 10.316 \text{ \AA}$; $\beta = 91.484^\circ$.

SUPPORTING INFORMATION

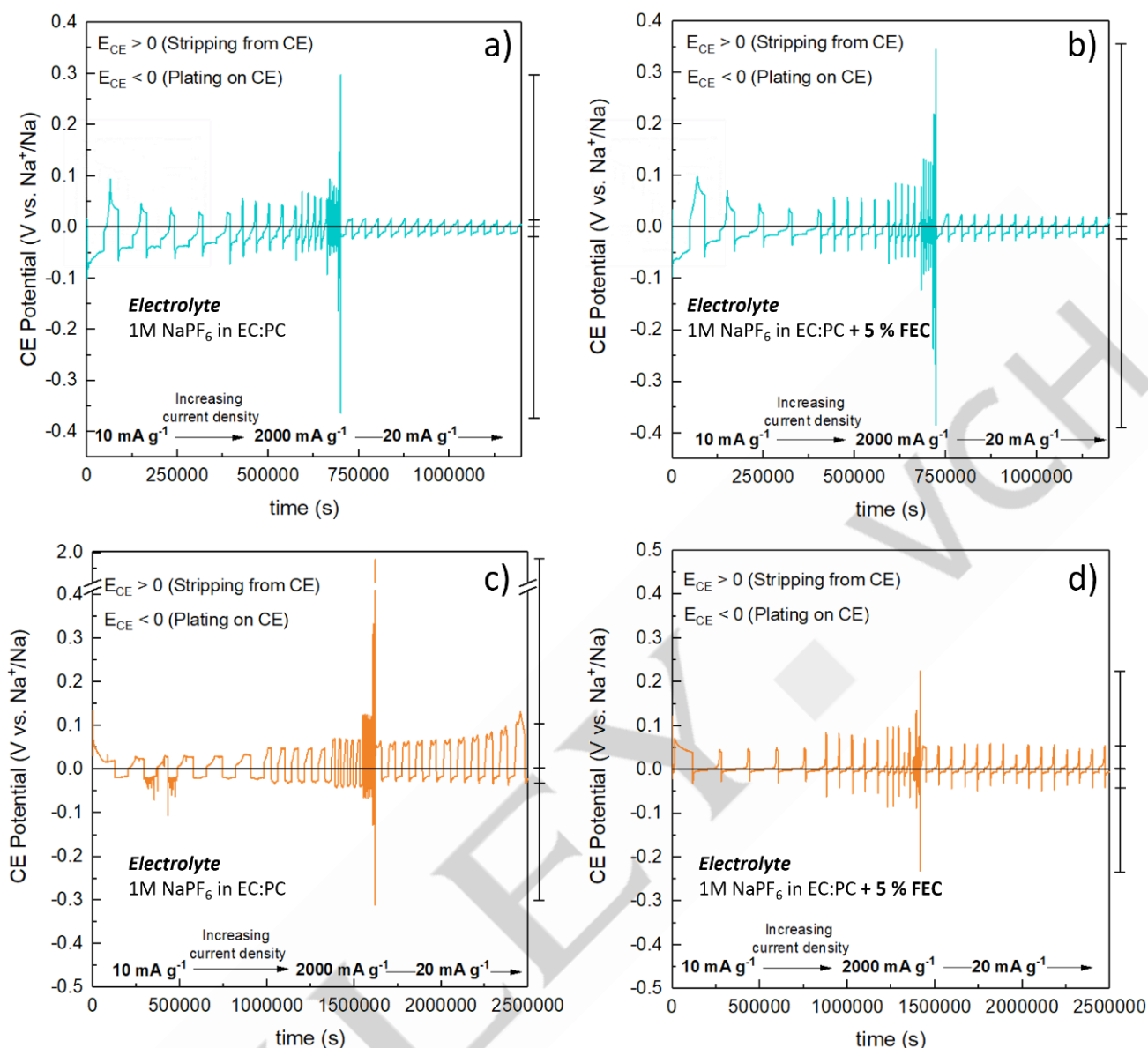


Figure S3. E_{CE} vs. t plot at different current densities (10, 20, 40, 100, 400, 1000 and 2000 mA g^{-1}) for half cells of NaMNMO a) without FEC and b) with FEC additive in the electrolyte; E_{CE} vs. t plot at different current densities (10, 20, 40, 100, 400, 1000 and 2000 mA g^{-1}) for half cells of CCDHC a) without FEC and b) with FEC additive in the electrolyte.

The obtained E_{CE} vs. t plots for half cells employing 1M NaPF_6 in EC:PC as the electrolyte were compared to half cells cycled with the addition of 5 % w/w FEC, as reported in **Figure S3**. By comparing the trend of the counter electrode potential upon cycling for cells without FEC (**Figure S3a,c**) and those with 5 % FEC in the electrolyte (**Figure S3b,d**), it is possible to observe that in the former case the sodium metal plating/stripping is not symmetrical for all current rates observed. This generally translates in an inhomogeneous deposition/dissolution of Na metal at the counter electrode side, which could result in the formation of dendrites during long-term cycling. After some cycling, this effect is visible for the NaMNMO cells even at slow rates (**Figure S3a-b**), and it is much more pronounced in the CCDHC cells especially at the higher current rates (**Figure S3c-d**).

SUPPORTING INFORMATION

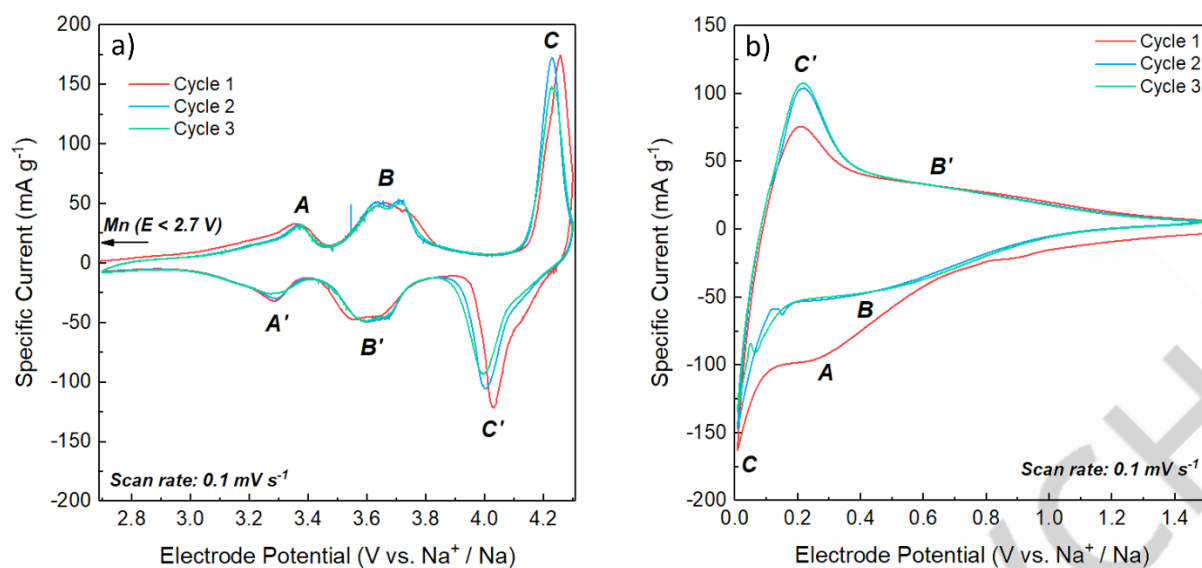


Figure S4. Cyclic voltammetry of the first three cycles at a scan rate of 0.1 mV s⁻¹ for a) NaMNMO and b) CCDHC.

Cathode: A = Ni^{2+/3+} oxidation
 B = Ni^{3+/4+} oxidation
 C = P2 to Z-phase transition

Anode: A = SEI formation
 B = Na⁺ ion adsorption
 C = Na⁺ ion intercalation

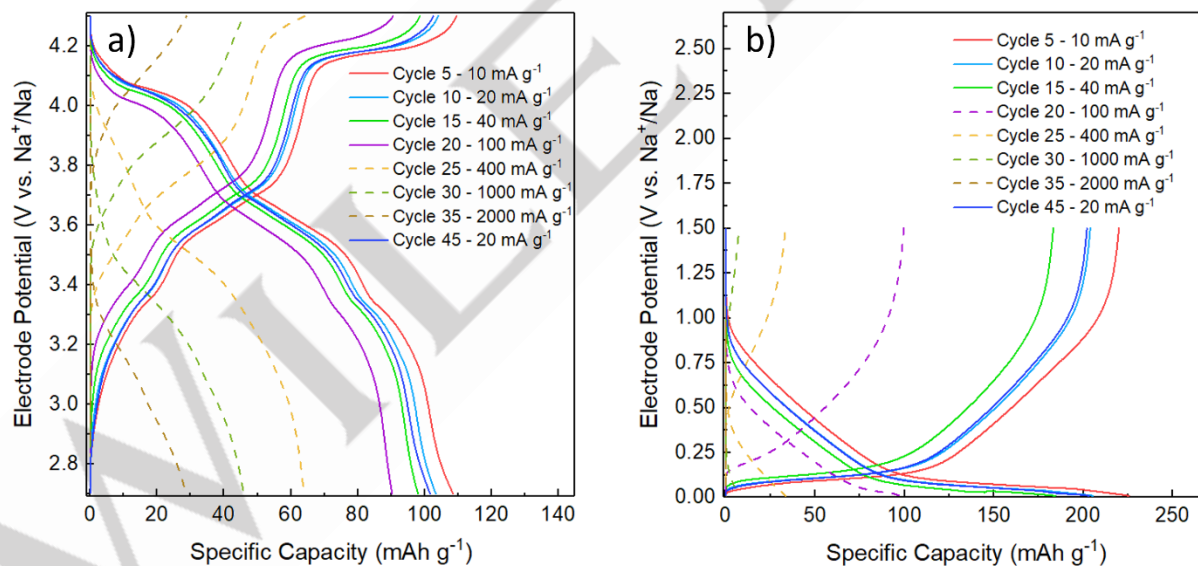


Figure S5. E vs. Q potential profiles for each specific current applied in the rate capability test for a) NaMNMO and b) CCDHC half cells.

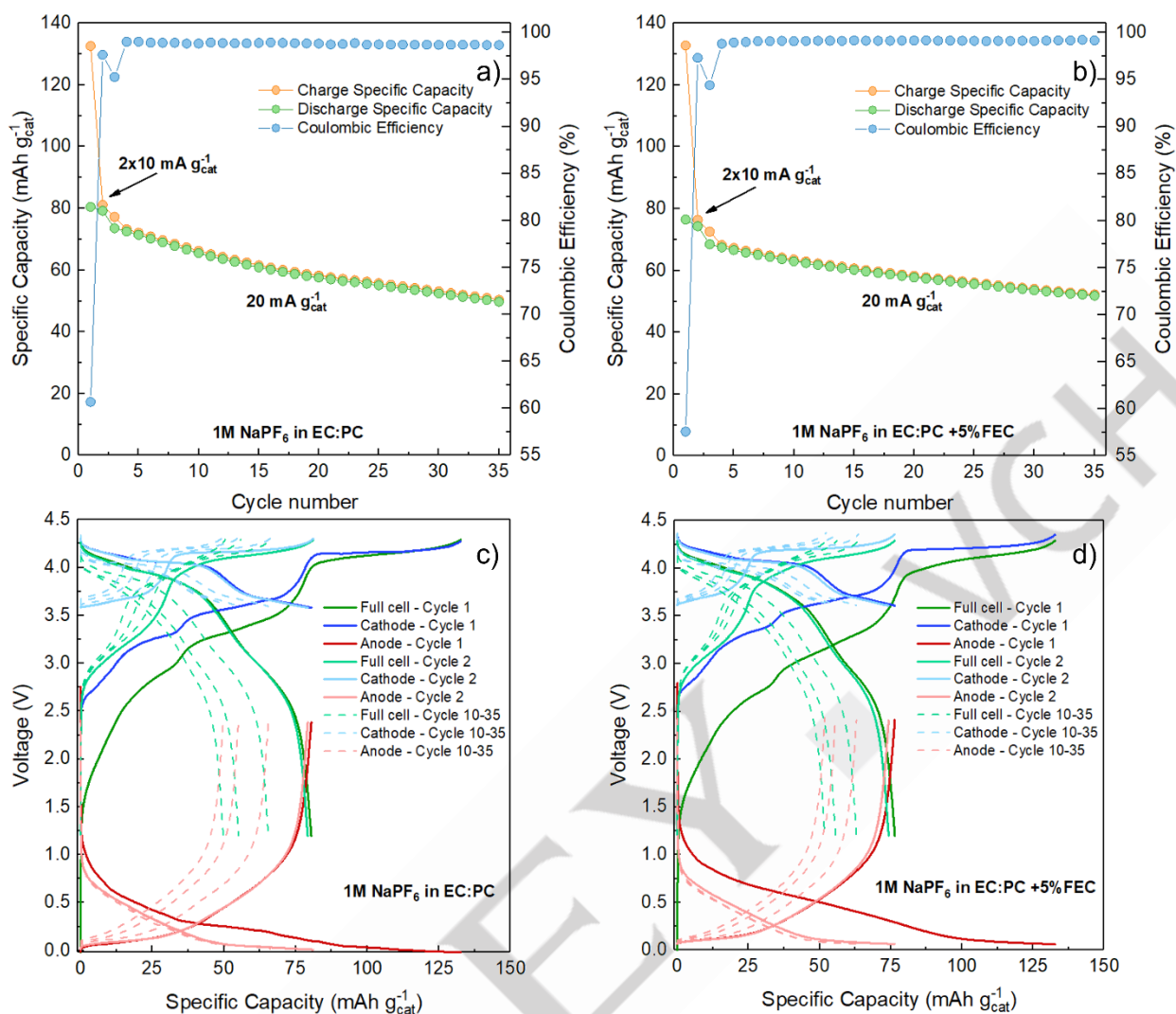


Figure S6. a) Galvanostatic cycles and c) E vs. Q potential profiles for the full cell employing standard NaPF₆ in EC:PC electrolyte; b) Galvanostatic cycles and d) E vs. Q potential profiles for the full cell employing NaPF₆ in EC:PC with 5 % FEC electrolyte. The applied current densities (20 mA g⁻¹ with two activation cycles at 10 mA g⁻¹) and specific capacities are normalized according to the mass of the cathode active material. The cathode and anode potentials (blue and red, respectively) are referred to the Na⁺/Na redox couple.

Both cells in **Figure S6a-b** display the same performance in terms of specific capacity, indicating that the use of FEC in the absence of metal Na at the counter electrode does not provide additional benefits. This is confirmed by comparing the potential profiles of the two cells as shown in **Figure S6c-d**, where no significant differences can be observed apart from the first charge; the slight difference in the first charge plateau in **Figure S6d** as compared to **Figure S6c** is due to the additional decomposition of FEC during the SEI formation at the anode, resulting in an increased irreversible consumption of sodium and a slightly lower initial coulombic efficiency.

SUPPORTING INFORMATION

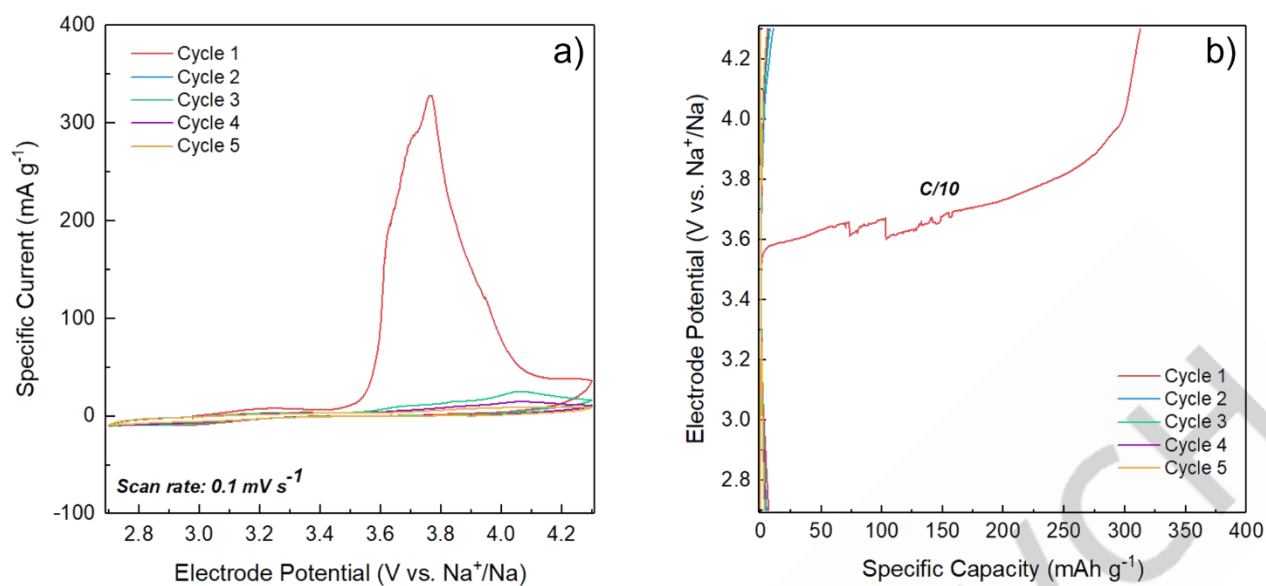


Figure S7. a) Cyclic voltammetry of five cycles at a scan rate of 0.1 mV s⁻¹ and b) E vs. Q potential profiles of five galvanostatic cycles obtained at C/10 C-rate ($Q_{th} = 339 \text{ mAh g}^{-1}$) for Na₂C₄O₄ half-cell. The electrolyte used for the measurement is 1M NaPF₆ EC:PC (1:1 mol/mol) + 5 % FEC.

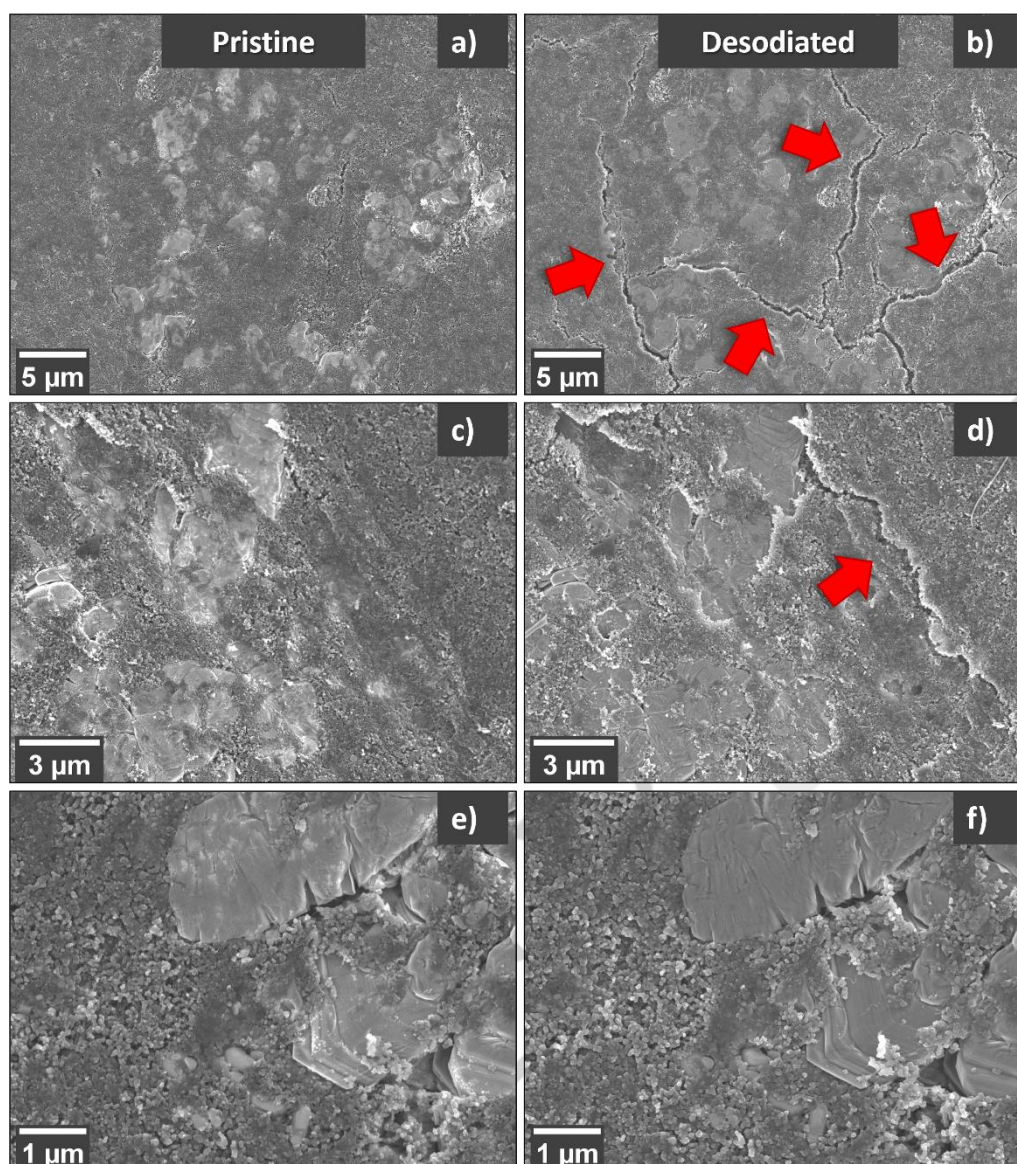


Figure S8. SEM micrographs of NaMnMO electrode at different magnifications and in different spots: a), c), e) pristine electrode before cycling and b), d), f) same sampling zones after the first desodiation in full cell configuration. Arrows indicate cracks formation.

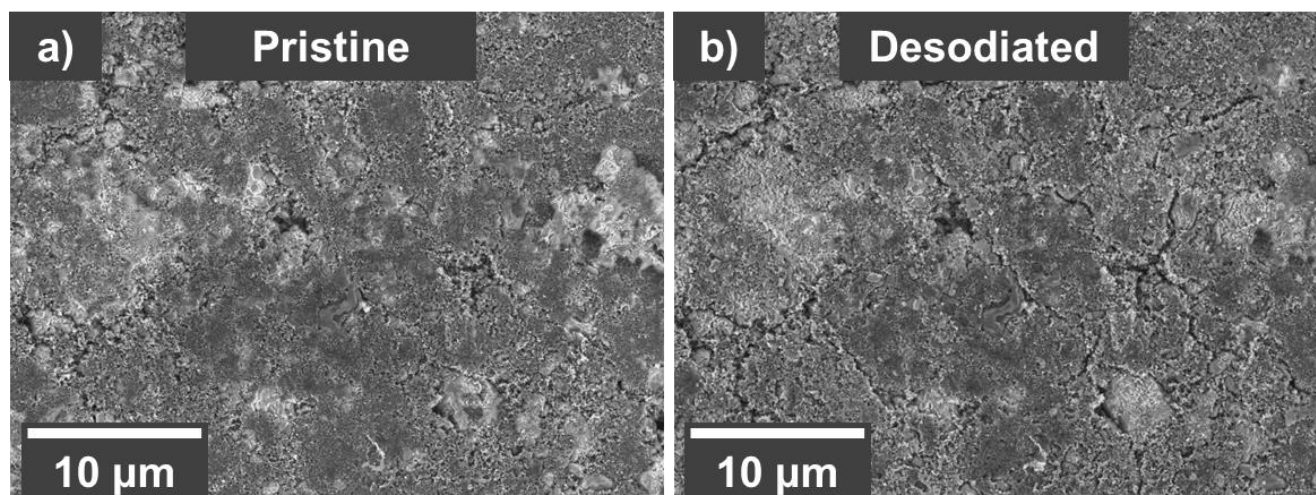


Figure S9. SEM micrographs of NaMnMO-SSq electrode at low magnification: a) pristine electrode before cycling and b) same sampling zone after the first desodiation in full cell configuration.

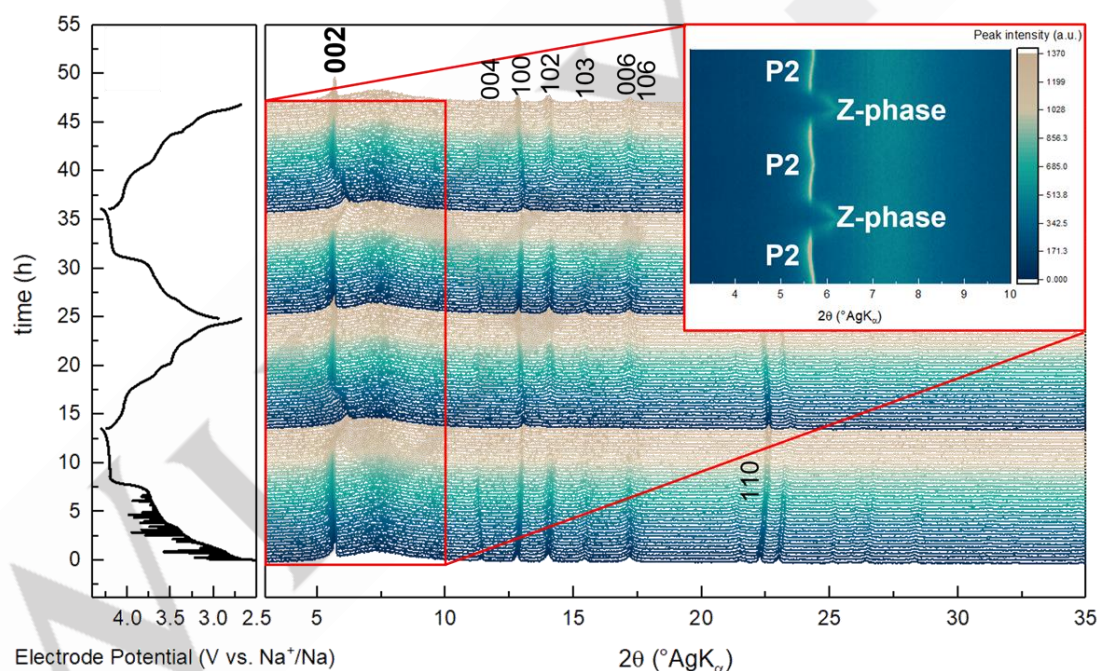


Figure S10. Operando XRD performed upon the first two cycles at 10 mA g^{-1} for NaMnMO half-cell. The inset shows a contour map highlighting the 002-reflection region associated to the P2 phase.

When charging within the $2.7 \text{ V} < E < 4.00 \text{ V}$ region, several structural changes can be observed, consistently with the electrochemical measurements. Specifically, during the initial charge, the 100, 102, 103 and 110 reflections are shifted to higher diffraction angles as the electrode potential increases, indicating an a -parameter contraction. A shift of the abovementioned reflections in the opposite direction is then observed, indicating an expansion of the a -parameter, and the repetition of this trend during the following cycle is consistent with a high reversibility of the structural transformations. The observed trend for the a -parameter upon cycling can be rationalized by considering the changes in the radius of the Ni-active metal ion being reversibly oxidized during desodiation to provide charge compensation within a solid solution regime. As opposed to the 10/ reflections, the 002 and 004 peaks are instead shifted to

SUPPORTING INFORMATION

lower diffraction angles upon charge, consistently with an expansion of the c -parameter. The trend of this parameter can be rationalized by considering that the extraction of sodium ions from the structure of the cathode results in a decrease of the positive charge stored between oxygen ions; hence, the repulsion between neighboring MO_2 slabs becomes stronger, and the interlayer distance ($d = c/2$) increases accordingly. When entering the high-voltage plateau region (about 4.2 V), the 002-reflection assigned to the P2 phase first remains at a constant position, and then starts decreasing until almost disappearing, indicating an almost complete phase transition. As the P2-related reflection starts to decrease, a new broadened reflection appears at higher diffraction angles, which has been reported to belong to the so-called OP4 phase for Mg-doped Ni-, Mn-based layered oxides. When approaching the 4.3 V cut-off, the reflection becomes broader and keeps shifting to higher angles, as a result of the increasing number of O2-type layers present in the structure. Given the continuous shifting of this reflection, the presence of several intermediate structures rather than only one specific OP4 structure is expected. Indeed, the extensive peak broadening is consistent with these intermediate structures existing at the same time. Therefore, the phase transition in the high-voltage region appears as an overall continuous process generally described as the “Z-phase”. Upon discharge, the P2-related reflection follows the opposite trend, rising back with the progressive disappearance of the Z-phase and a contraction of the c -parameter due to the shielding of the repulsion between neighboring MO_2 slabs given by the inserted sodium ions. This behavior is also repeated during the subsequent cycle, indicating a high reversibility of the phase transition. It is worth noting that the lattice parameter of the P2-related reflection (i.e. 002) stops changing around 3.7 V. This occurs before the P2 \rightarrow Z-phase transition takes place, possibly leading to a pseudocapacitive region with Na^+ /vacancy ordering. This phenomenon has been observed for similar doped layered oxides, and is evidenced by a flat high-voltage plateau.

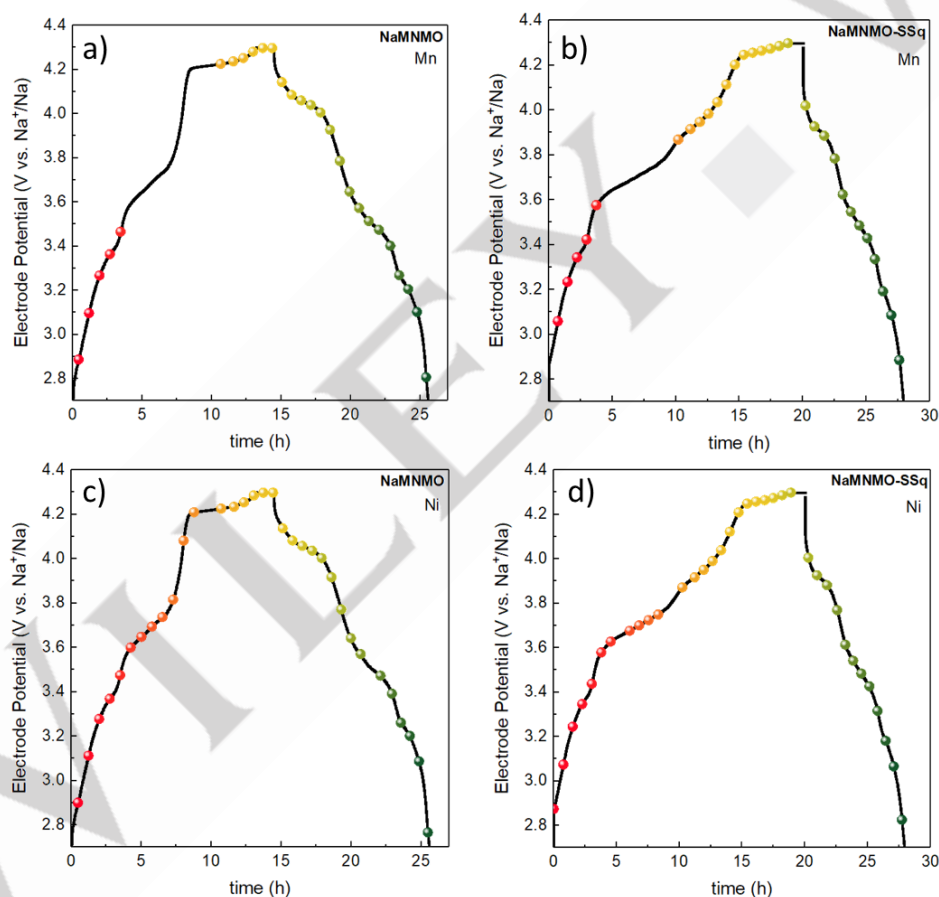


Figure S11. Galvanostatic profiles for the operando cells indicating the acquisition points for a) Mn in NaMnMO, b) Mn in NaMnMO-SSq, c) Ni in NaMnMO and d) Ni in NaMnMO-SSq.

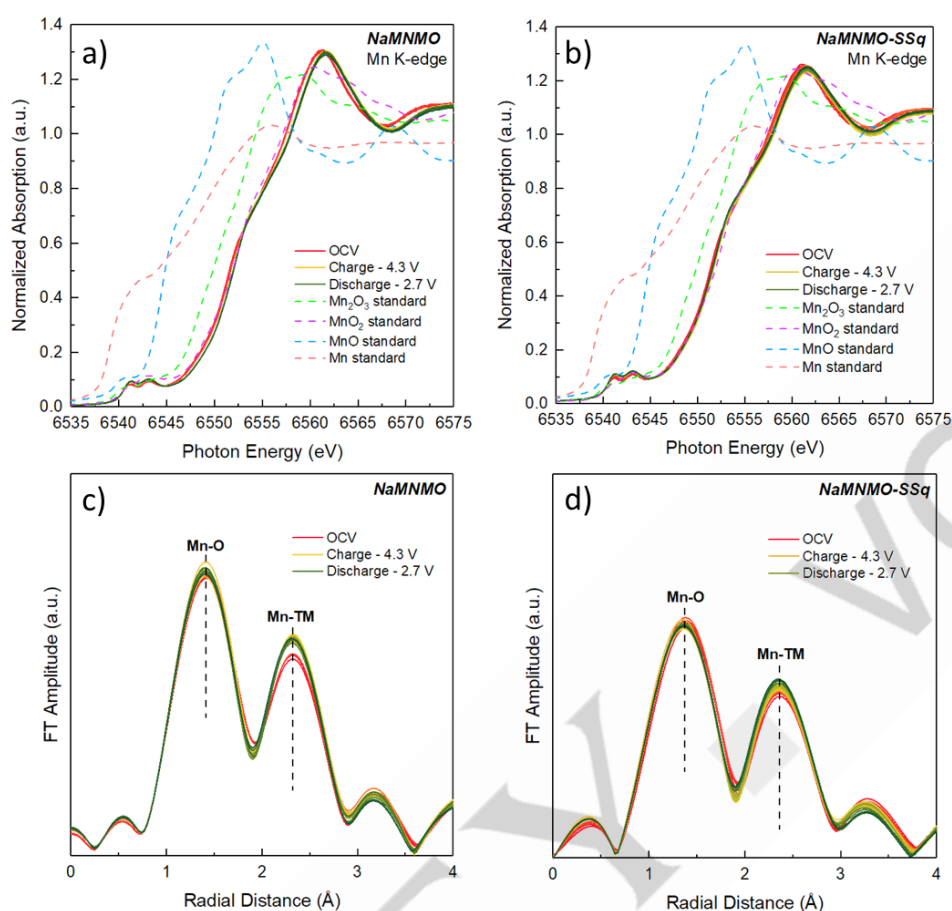


Figure S12. XANES spectra at Mn K-edge for a) NaMnMO and b) NaMnMO-SSq; corresponding EXAFS spectra for c) NaMnMO and d) NaMnMO-SSq. The colors for the spectra at different potentials correspond to those indicated in the galvanostatic profiles (see **Figure S11**).

The Mn K-edge in the X-ray absorption near edge structure (XANES) is consistent with Mn being in +4 oxidation state, and it never shifts during cycling, thus indicating that the oxidation state of Mn does not change, as expected by cutting the Mn⁴⁺/Mn³⁺ redox couple activity out of the chosen voltage window. The extended X-ray absorption fine structure (EXAFS) spectra further confirm this result when considering the shells at 1.4 Å and 2.3 Å (representing the Mn-O and Mn-TM interactions, respectively). Indeed, for both systems the interatomic distances never change upon cycling, indicating that the fine structure of Mn stays unchanged. Moreover, the decomposition of the sacrificial salt does not seem to affect the local structure of Mn, as the two systems display the same behavior upon cycling.

SUPPORTING INFORMATION

Table S1. Atomic weight fractions for in-house XPS measurements on NaMnMO, NaMnMO-SSq and CCDHC electrodes before and after one galvanostatic cycle in full cell configuration.

| | | NaMnMO | | | CCDHC | | |
|-------------|--|----------|--------|--------------|----------|--------|--------------|
| | | Pristine | 1cycle | 1cycle (SSq) | Pristine | 1cycle | 1cycle (SSq) |
| C1s | sp ² | 55.3 | 49.1 | 4.6 | 27.8 | 1.8 | |
| | C-H | 5.0 | | 7.3 | 36.5 | 35.2 | 18.0 |
| | -C-O | | 4.6 | 22.7 | 10.5 | 3.5 | 18.5 |
| | -CH-CF ₂ | 7.6 | 8.3 | | | | |
| | -CO ₂ | | | 6.8 | 2.2 | 4.6 | 5.1 |
| | -CO ₃ | | | 6.2 | | 3.0 | 5.6 |
| | -CF ₂ | 9.0 | 8.42 | | | | |
| | charge | | | 0.7 | | 2.4 | 1.3 |
| O1s | MO | 0.1 | | | | | |
| | -C-O | 0.4 | 2.8 | 13.6 | 7.4 | 6.8 | 13.4 |
| | -C=O | 1.1 | 2.1 | 12.6 | 8.9 | 11.6 | 16.0 |
| F1s | -CF ₂ | 20 | | | | | |
| | NaPF ₆ | | 21.7 | 14.5 | 1.0 | 18.5 | 12.2 |
| | NaF | 0.6 | 0.6 | | | 0.4 | |
| | charge | | | 2.7 | | 1.0 | |
| P2p | NaPF ₆ | | 1.0 | 0.9 | | 2.4 | 2.2 |
| | Na _x PF _y O _z | | | | | | |
| Na1s | | | 0.4 | 4.4 | 1.4 | 8.8 | 4.9 |
| Mn2p | | | | | | | |
| Mg2s | | 0.1 | | | | | |
| Si2p | | 0.2 | 0.1 | 0.1 | | | 0.6 |
| Cl2p | | 0.4 | 0.7 | | | | |
| K2p | | | | | 3.6 | | |
| S2p | | | | | 0.6 | | |

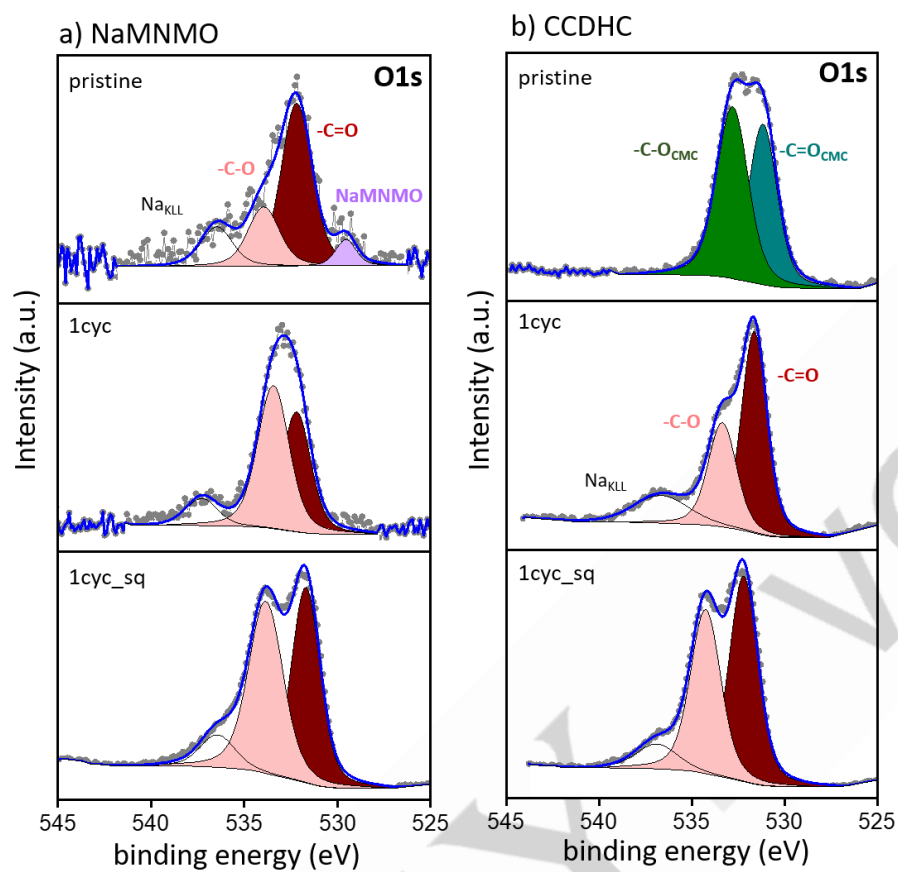


Figure S13. O1s XPS spectra of a) NaMNMO and b) CCDHC electrodes. The pristine samples (top) refer to electrodes without SSq, prior to cycling. Electrodes with and without SSq additive were measured after 1 cycle (middle and bottom).

SUPPORTING INFORMATION

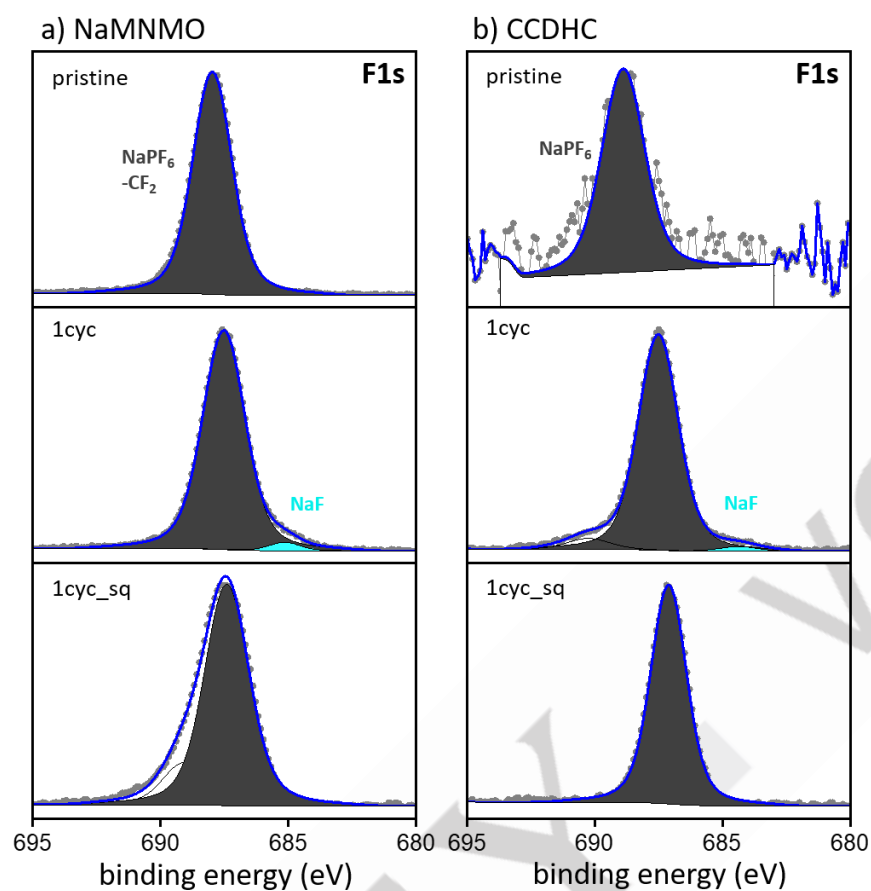


Figure S14. F1s XPS spectra of a) NaMnMO and b) CCDHC electrodes. The pristine samples (top) refer to electrodes without SSq, prior to cycling. Electrodes with and without SSq additive were measured after 1 cycle (middle and bottom).

Table S2. Peak frequencies obtained from DRT calculations for P2 and P3 of CCDHC||NaMnMO and CCDHC||NaMnMO-SSq full cells, at the first cycle and after 92 galvanostatic cycles.

| Peak | Cycle number | CCDHC NaMnMO | CCDHC NaMnMO-SSq |
|-----------|-----------------|---------------------------|---------------------------------------|
| <i>P2</i> | Cycle 1 | 10 Hz < <i>f</i> < 100 Hz | <i>f</i> < 10 Hz |
| | Cycle 92 | <i>f</i> ~ 100 Hz | <i>f</i> ~ 10 Hz |
| <i>P3</i> | Cycle 1 | 0.1 Hz < <i>f</i> < 1 Hz | 0.1 Hz < <i>f</i> < 1 Hz |
| | Cycle 92 | 0.01 < <i>f</i> < 0.1 Hz | <i>f</i> < 0.01 Hz |

Data availability

The data that support the findings of this study are openly available at <https://doi.org/10.5281/zenodo.10161577>.